

Verification of 1-D Transcritical Flow Model in Channels

MING-HSENG TSENG

*Engineering Applied Research II
National Center for High-Performance Computing
Hsinchu, Taiwan, R.O.C.*

(Received November 30, 1998; Accepted March 22, 1999)

ABSTRACT

This paper deals with the use of high-resolution non-oscillatory shock-capturing difference schemes to solve steady and unsteady one-dimensional flows with steep waves in channels. Such transcritical flow may be either free surface (subcritical/supercritical) or free surface/pressurized in a pipe. The main features of a class of high-resolution schemes are described with reference to the unsteady one-dimensional shallow water equations. The operator splitting method is utilized to compute the flows with bottom slope and friction terms, and the method of characteristics with second-order accuracy is also incorporated in the present model to treat the external and internal boundary conditions. Numerical results are obtained for a series of one-dimensional test cases by means of the proposed model and are compared with analytical solutions or experimental measurements. It is shown that the proposed model is accurate, robust and highly stable in capturing strong gradients and discontinuities in such transcritical flows, and is a reliable mathematical model for one-dimensional practical hydraulic engineering applications.

Key Words: high-resolution non-oscillatory shock-capturing difference schemes, unsteady one-dimensional shallow water equations, transcritical flows

I. Introduction

Transcritical flow or an abrupt change in water depth often occurs in channels. The resulting flow may be a subcritical/supercritical free surface flow or a free surface/pressurized flow if the channel is closed (pipe). For example, the operation of fixed and dynamic hydraulic structures sometimes leads to the formation of shock, that is, hydraulic jumps or surges. Other occurrences of transcritical flow include dam-break waves and flow through channels with severe width contractions or local high-bed elevations. The mathematical modeling of transcritical flow is an extremely difficult problem due to the presence of rapidly varying discontinuous hydraulic characteristics.

A number of shock-capturing finite difference schemes exists for solving hyperbolic systems of conservation laws in the field of aerodynamics. Because the 1-D shallow water equations are similar to the 1-D compressible Navier-Stokes equations, many works in the last decade have focused on the numerical solution of the de Saint Venant equations and have mainly attempted to accurately capture discontinuities without spurious oscillations. Fennema and Chaudhry (1987, 1990) used the Beam and Warming scheme and the

MacCormack scheme to simulate one and two-dimensional dam-break flows. An important feature is the requirement of additional artificial dissipation terms in order to remove oscillations around discontinuities using these classical higher-order schemes. This requires good judgement and empiricism. Roe (1981) defined an approximate Jacobian for conservative splitting of the flux difference in Euler equations. Harten (1983) introduced the total variation diminishing (TVD) schemes, which have the ability not only to damp oscillations, but also to highly resolve discontinuities, and which contain no terms depending on adjustable parameters. The Roe scheme and TVD schemes were employed to solve the one-dimensional transcritical flow in many researches (Glaister, 1988; Alcrudo *et al.*, 1992; Baines *et al.*, 1992; Yang *et al.*, 1993; Nujic, 1995; Jha *et al.*, 1995; Jin and Fread, 1997; Meselhe *et al.*, 1997). Because the TVD schemes are required to revert to first-order at the local extrema of the solutions, Harten and Osher (1987) developed the essentially non-oscillatory (ENO) schemes, which are able to achieve uniformly higher-order accuracy both at the local extrema of the solutions and in other smooth regions. The ENO schemes were extended to solve the one-dimensional dam-break problem by a few inves-

tigators (Yang *et al.*, 1993; Nujic, 1995). Although the previous researches reported good results near discontinuities, most of them were proposed for only the prismatic channel, or neglected the source terms, and some of them used only first-order scheme, or required tuning of the artificial viscosity coefficient.

Recently, Tseng (1999) applied a class of non-oscillatory shock-capturing Roe, TVD, and ENO schemes to the simulation of two-dimensional rapidly varied open-channel flows. His results demonstrated that the above schemes are accurate, robust and highly stable even in flows with strong gradients. In this paper, these high-resolution explicit schemes are extended to solve the one-dimensional transcritical flow. Also, the entropy correction function suggested by Harten and Hyman (1983) is used to eliminate the trial procedure for the entropy inequality condition. At boundaries, the method of characteristics with second-order accuracy is also incorporated in the present schemes to treat the time-dependent hydraulic engineering problem. To verify the reliability of the proposed model for hydraulic engineering applications, a series of test cases are presented, and simulation results are compared with the analytical solution or experimental data.

The contents of this paper are organized as follows. Governing equations are described in Section II. The numerical model is presented in Section III. In Section IV, several one-dimensional, steady and unsteady, rapidly varying, transcritical flow computations are used to validate and demonstrate the accurate, robust and stable features of the proposed model. Finally, conclusions are given in the last section.

II. Governing Equations

Under the assumption of a homogeneous, incompressible, viscous flow characterized by a hydrostatic pressure distribution, with wind and Coriolis forces neglected, the depth-integrated equations of motion form the fundamental equations for open-channel flows. The governing equations, based on conservation of mass and of momentum, for one-dimensional unsteady flow in a nonprismatic channel of arbitrary cross section, can be expressed as

$$\frac{\partial Q}{\partial t} + \frac{\partial F}{\partial x} = S, \quad (1)$$

in which

$$Q = \begin{pmatrix} A \\ Q \end{pmatrix}, \quad F = \begin{pmatrix} Q \\ Q^2 A^{-1} + g I_1 \end{pmatrix},$$

$$S = \begin{pmatrix} 0 \\ g I_2 + g A (S_0 - S_f) \end{pmatrix},$$

where t is time; x is the horizontal distance along the channel; A is the wetted cross-sectional area; Q is the volume rate of flow; g is the gravitational acceleration; and S_0 is the bed slope. The frictional slope S_f , the hydrostatic pressure force I_1 , and the pressure force due to longitudinal width variation I_2 are defined as

$$S_f = \frac{Q |Q| n^2}{A^2 R^{4/3}}, \quad I_1 = \int_0^{h(x,t)} (h - \eta) b(x, \eta) d\eta, \\ I_2 = \int_0^{h(x,t)} (h - \eta) \frac{\partial b(x, \eta)}{\partial x} d\eta, \quad (2)$$

where $b(x, \eta) = \partial A(x, \eta) / \partial \eta$; h = total water depth; n = the Manning's roughness coefficient; and R = the hydraulic radius.

If channel cross sections are rectangular, triangular or trapezoidal, the I_1 and I_2 terms can be expressed as

$$I_1 = h^2 \left(\frac{B}{2} + \frac{h S_L}{3} \right), \quad I_2 = h^2 \left(\frac{1}{2} \frac{dB}{dx} + \frac{h}{3} \frac{dS_L}{dx} \right), \quad (3)$$

where B is the channel bottom width, and S_L is the side slope of the channel (vertical to horizontal). The notations of a trapezoidal cross section are shown in Fig. 1.

Equation (1) can be further expressed in quasi-linear form as

$$\frac{\partial Q}{\partial t} + A \frac{\partial Q}{\partial x} = S, \quad A = \frac{\partial F}{\partial Q}, \quad (4)$$

where A is the Jacobian matrix and has two real eigenvalues:

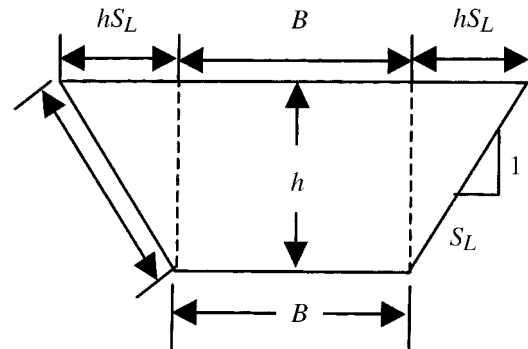


Fig. 1. Notations of a trapezoidal cross section.

$$\lambda_1 = \frac{Q}{A} + c, \text{ and } \lambda_2 = \frac{Q}{A} - c, \quad (5)$$

in which $c (= \sqrt{gA/T})$ is the wave celerity, and T is the water surface width.

The corresponding right and left eigenvector matrices for A are

$$\mathbf{R} = \frac{1}{2c} \begin{pmatrix} 1 & -1 \\ \lambda_1 & -\lambda_2 \end{pmatrix}, \quad \mathbf{L} = \begin{pmatrix} -\lambda_2 & 1 \\ -\lambda_1 & 1 \end{pmatrix}. \quad (6)$$

Due to the hyperbolicity, we have

(7)

Free surface/pressurized flow conditions may also be considered in a pipeline by introducing the Preissmann's slot (Cunge *et al.*, 1980) attached to the pipe crown and over the entire length of the pipe. The result is still a free surface flow, but since the wave speed is $\sqrt{gA/B_S}$, where B_S is the channel width at the free surface, pressurized flow with a large wave speed is simulated as the water level enters the slot.

III. Numerical Model

1. Roe/TVD/ENO Schemes

Define a uniform mesh $\{x_j, t^n\}$, with mesh size Δx , time increment Δt and $\tau = \Delta t / \Delta x$, called the mesh ratio. A conservative scheme for Eq. (1), with the source term omitted temporarily, can be written as

$$\mathbf{Q}_j^{n+1} = \mathbf{Q}_j^n - \tau [\tilde{\mathbf{F}}_{j+\frac{1}{2}} - \tilde{\mathbf{F}}_{j-\frac{1}{2}}], \quad (8)$$

where $\tilde{\mathbf{F}}_{j+\frac{1}{2}}$ and $\tilde{\mathbf{F}}_{j-\frac{1}{2}}$ are the so-called modified numerical fluxes.

The first-order Roe scheme (Roe, 1981) and higher-order schemes (Harten, 1983; Harten and Osher, 1987; Hsu, 1995), including the second-order TVD and ENO schemes and the third-order ENO scheme, can be expressed in the form of Eq. (8) by defining the modified numerical flux as

$$\tilde{\mathbf{F}}_{j+\frac{1}{2}} = \frac{1}{2} [\mathbf{F}_j + \mathbf{F}_{j+1} + \mathbf{R}_{j+\frac{1}{2}} \boldsymbol{\Phi}_{j+\frac{1}{2}}]. \quad (9)$$

The components of $\boldsymbol{\Phi}_{j+\frac{1}{2}}$ are defined as

$$\phi_{j+\frac{1}{2}}^l = \mu(e_j^l + e_{j+1}^l) \sigma(\lambda_{j+\frac{1}{2}}^l) + \theta(d_j^l + d_{j+1}^l) \bar{\sigma}(\lambda_{j+\frac{1}{2}}^l)$$

$$- \Psi(\lambda_{j+\frac{1}{2}}^l + \mu \gamma_{j+\frac{1}{2}}^l + \theta \delta_{j+\frac{1}{2}}^l) \alpha_{j+\frac{1}{2}}^l, \quad l=1, 2, \quad (10)$$

where $\alpha_{j+\frac{1}{2}}^l$ represents the characteristic variables, defined as²

$$\alpha_{j+\frac{1}{2}}^l = \mathbf{L}_{j+\frac{1}{2}} (\mathbf{Q}_{j+1} - \mathbf{Q}_j), \quad (11)$$

and other higher-order terms are given by

$$\sigma(z) = \frac{1}{2} [\varphi(z) - \tau z^2], \quad (12)$$

$$\bar{\sigma}(z) = \begin{cases} (\tau^2 |z|^3 - 3\tau |z|^2 + 2|z|)/6, & \text{if } |\alpha_{j-\frac{1}{2}}^l| \leq |\alpha_{j+\frac{1}{2}}^l| \\ (\tau^2 |z|^3 - |z|)/6, & \text{otherwise,} \end{cases} \quad (13)$$

and

$$e_j^l = m[\alpha_{j+\frac{1}{2}}^l - \beta \bar{m} (\Delta_- \alpha_{j+\frac{1}{2}}^l, \Delta_+ \alpha_{j+\frac{1}{2}}^l), \alpha_{j-\frac{1}{2}}^l + \beta \bar{m} (\Delta_- \alpha_{j-\frac{1}{2}}^l, \Delta_+ \alpha_{j-\frac{1}{2}}^l)], \quad (14)$$

$$d_j^l = \begin{cases} \bar{m} (\Delta_- \alpha_{j-\frac{1}{2}}^l, \Delta_+ \alpha_{j-\frac{1}{2}}^l), & \text{if } |\alpha_{j-\frac{1}{2}}^l| \leq |\alpha_{j+\frac{1}{2}}^l| \\ \bar{m} (\Delta_- \alpha_{j+\frac{1}{2}}^l, \Delta_+ \alpha_{j+\frac{1}{2}}^l), & \text{otherwise,} \end{cases} \quad (15)$$

$$\gamma_{j+\frac{1}{2}}^l = \begin{cases} \sigma(\lambda_{j+\frac{1}{2}}^l) (e_{j+1}^l - e_j^l) / \alpha_{j+\frac{1}{2}}^l, & \text{if } \alpha_{j+\frac{1}{2}}^l \neq 0 \\ 0, & \text{otherwise,} \end{cases} \quad (16)$$

$$\delta_{j+\frac{1}{2}}^l = \begin{cases} \bar{\sigma}(\lambda_{j+\frac{1}{2}}^l) (d_{j+1}^l - d_j^l) / \alpha_{j+\frac{1}{2}}^l, & \text{if } \alpha_{j+\frac{1}{2}}^l \neq 0 \\ 0, & \text{otherwise.} \end{cases} \quad (17)$$

In the above expressions, z is a dummy variable; Δ_+ is the forward difference; Δ_- is the backward difference; the limiter functions m and \bar{m} are defined as

$$m(a, b) = \begin{cases} s \min(|a|, |b|), & \text{if } \text{sgn } a = \text{sgn } b = s; \\ 0, & \text{otherwise,} \end{cases} \quad (18)$$

$$\overline{m}(a,b) = \begin{cases} a, & \text{if } |a| \leq |b|; \\ b & \text{otherwise,} \end{cases} \quad (19)$$

and the entropy fix function φ is

$$\varphi(z) = \begin{cases} |z|, & \text{if } |z| \geq \varepsilon; \\ (z^2 + \varepsilon^2)2\varepsilon, & \text{if } |z| < \varepsilon, \end{cases} \quad (20)$$

in which ε is a small positive number whose value has to be determined for each individual problem. In this paper, a formula suggested by Harten and Hyman (1983) is used to cut down trial process:

$$\left. \begin{aligned} \varepsilon_{j+\frac{1}{2}}^l &= \max [0, \lambda_{j+\frac{1}{2}}^l - \lambda_j^l, \lambda_{j+1}^l - \lambda_{j+\frac{1}{2}}^l] \\ \varepsilon_{j-\frac{1}{2}}^l &= \max [0, \lambda_{j-\frac{1}{2}}^l - \lambda_{j-1}^l, \lambda_j^l - \lambda_{j-\frac{1}{2}}^l] \end{aligned} \right\} \quad (21)$$

In the above equations, the three parameters μ , θ and β are used to enable the first-order Roe scheme (ROE1), the second-order TVD scheme (TVD2), the second-order ENO scheme (ENO2) and the third-order ENO scheme (ENO3) to be expressed in the same formulations. In addition, the relations are

$$\left. \begin{aligned} \mu=0 \quad \theta=0 \quad \beta=0 &\rightarrow \text{ROE1} \\ \mu=1 \quad \theta=0 \quad \beta=0 &\rightarrow \text{TVD2} \\ \mu=1 \quad \theta=0 \quad \beta=0.5 &\rightarrow \text{ENO2} \\ \mu=1 \quad \theta=1 \quad \beta=0 &\rightarrow \text{ENO3} \end{aligned} \right\} \quad (22)$$

The subscript $j\pm 1/2$ denotes the intermediate state between grid points j and $j+1$, and can be defined following the lead of Roe (1981) as

$$\begin{aligned} u_{j\pm\frac{1}{2}} &= \frac{\sqrt{A_j}u_j + \sqrt{A_{j\pm 1}}u_{j\pm 1}}{\sqrt{A_j} + \sqrt{A_{j\pm 1}}}, \quad h_{j\pm\frac{1}{2}} = (h_j + h_{j\pm 1})/2, \\ c_{j\pm\frac{1}{2}} &= \sqrt{\frac{gA(h_{j\pm\frac{1}{2}})}{T(h_{j\pm\frac{1}{2}})}}. \end{aligned} \quad (23)$$

A special situation arises in the case of a wave tip overrunning a dry bed. For this case, the values $u_{j\pm 1/2}=u_j$ and $c_{j\pm 1/2}=0$ are used.

For Eq. (1) with a non-zero source term, the operator splitting technique (Strang, 1968) is employed to maintain in the above schemes uniform second-order accuracy, and the resulting method can be expressed as

$$\left. \begin{aligned} \mathbf{Q}_j^{n+1} &= L_s(\frac{\Delta t}{2})\mathbf{L}(\Delta t)L_s(\frac{\Delta t}{2})\mathbf{Q}_j^n \\ L(\Delta t)\mathbf{Q}_j^n &\equiv \mathbf{Q}_j^n - \tau[\tilde{\mathbf{F}}_{j+\frac{1}{2}}^n - \tilde{\mathbf{F}}_{j-\frac{1}{2}}^n] \\ L_s(\Delta t)\mathbf{Q}_j^n &\equiv \mathbf{Q}_j^n + \Delta t\mathbf{S}_j^n + \frac{\Delta t^2}{2}(\frac{\partial \mathbf{S}}{\partial \mathbf{Q}})_j^n \mathbf{S}_j^n \end{aligned} \right\} \quad (24)$$

For stability in an explicit scheme, the Courant-Friedrichs-Lewy condition must be satisfied; i.e., the Courant number C_r must be less than or equal to unity. In other words, the time increment Δt is limited as follows:

$$\Delta t = C_r \left[\frac{\Delta x}{u+c} \right]. \quad (25)$$

2. Boundary Conditions

The above schemes are only for the interior points. If one of the flow variables is prescribed at one of the boundary sections, then a solution for the other dependent variable is still needed. It should be recalled that the only general technique available to obtain a solution to this problem is the method of characteristics (MOC). In this paper, second-order accuracy boundary conditions based on the method of characteristics are employed at the boundaries. For subcritical flows, one external condition must be specified at the inflow boundary whereas the other is required at the outflow boundary, and the remaining unknown variables on both sides are furnished by the MOC. Supercritical flows require the imposition of two inflow boundary conditions, and all the variables at the downstream side are solved by the MOC.

The characteristic equations for Eq. (1) may be written as

$$\frac{dQ}{dt} + \left(-\frac{Q}{A} \pm \sqrt{\frac{gA}{T}} \right) \frac{dA}{dt} = gI_2 + gA(S_0 - S_f), \quad (26)$$

which are known to hold along characteristic lines:

$$\frac{dx}{dt} = \frac{Q}{A} \pm \sqrt{\frac{gA}{T}}. \quad (27)$$

The first equation (C_+ , forward) is used at the end of the reach, the second (C_- , backward) at the inlet. Since a fixed grid is being considered, a proper spatial interpolation is needed in the numerical evaluation of the integrals in Eqs. (26) and (27). In this paper, the Hartree method (Liggett and Cunge, 1975; Garcia-Navarro and Saviron, 1992) is employed to achieve second-order accuracy for boundary point solutions.

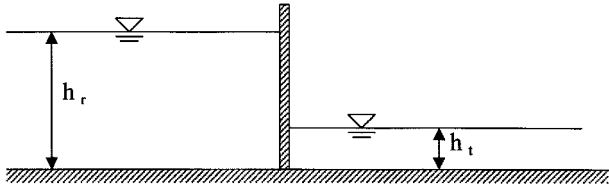


Fig. 2. Schematic diagram of a dam-break flow.

IV. Model Applications

In this section, numerical simulations of several one-dimensional transcritical flows, including dam-break flows under both wet and dry bed conditions, pressurization in a single pipe, a hydraulic jump application and steady flow over a ladder of weirs, are presented to validate and demonstrate the robustness and accuracy of the proposed model. In all cases, the grid systems are designed so as to be fine enough to meet the requirements of adequate accuracy as well as reasonable execution time.

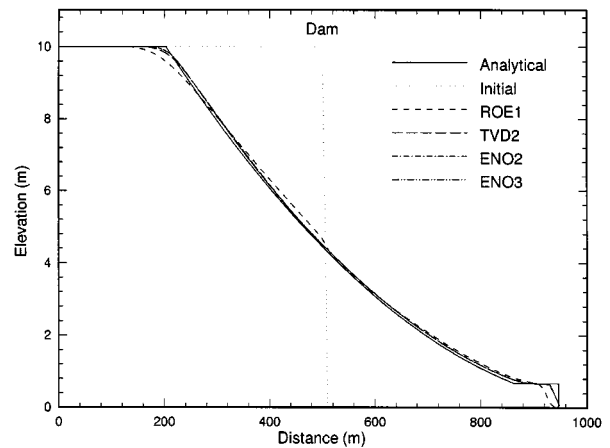
1. Idealized Dam-Break Flow on Wet and Dry Beds

The first test case for the present schemes is an idealized dam-break flow in a rectangular, frictionless channel. Figure 2 shows a schematic diagram of the problem, where h_r and h_t are the initial water depths in the reservoir and in the tail water, respectively. At time $t=0$, the dam is removed instantly, and water is released into the downstream side in the form of a shock wave. Based on the geometry and upstream conditions, an analytic solution can be found. The flow can be subcritical or supercritical, depending on the depth ratio (h_t/h_r). The value of the depth ratio is largely responsible for the problems encountered in simulating the dam-break flow. The severity of the problem increases as the depth ratio decreases. Fennema and Chaudhry (1987) showed that if the depth ratio is less than 0.05, then most numerical schemes do not give accurate results at the bore. In this study, the computational domain was comprised of a 1000 m long channel with a horizontal channel bottom. The dam was located at a downstream distance of $x=500$ m. The initial water depth in the reservoir was $h_r=10$ m. Time evolution of the water depth could be used to examine the shock-capturing capability of the numerical scheme.

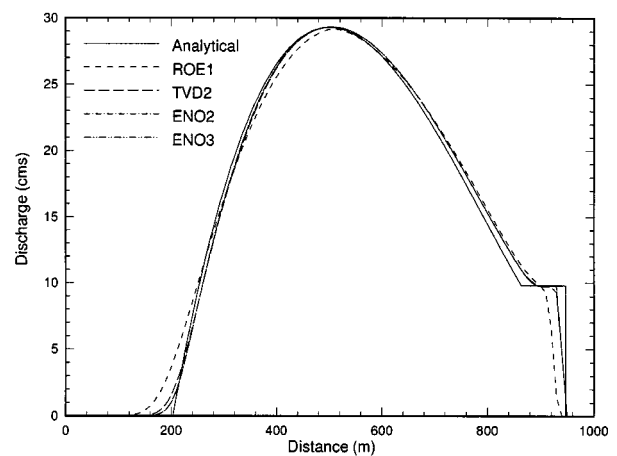
Figure 3(a) shows the variation of the water depth along the channel for a dam-break flow with a depth ratio $h_t/h_r=0.001$ at time $t=30$ sec. The flow domain was discretized into 100 uniform grids, and the ROE1, TVD2, ENO2, and ENO3 schemes with $C_r=1$ were adopted. The analytical solutions were obtained using

Stoker's solution (Stoker, 1957). The simulated water surface profiles follow closely the analytical solution for both the positive and negative waves except for the ROE1 scheme, which is only a first-order scheme and has significant numerical damping, leading to stronger smearing of the discontinuities and slower shock movement. A comparison of the computed and analytical discharge profiles is shown in Fig. 3(b). The excellent match reveals the mass conservation characteristic of the TVD2, ENO2 and ENO3 schemes. Since the ROE1 scheme has only first-order accuracy, significant differences from the other three schemes are exhibited.

The study of a flood wave due to sudden failure of a hydraulic structure over an initially dry bed may be important. In this test, the water surface and discharge profiles with a dry bed downstream ($h_t/h_r=0.0$),



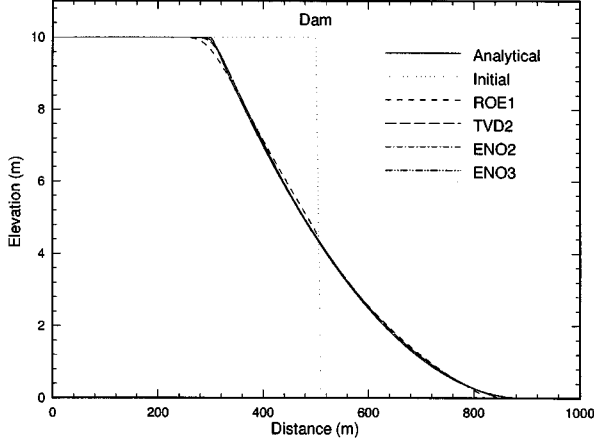
(a) Water depth



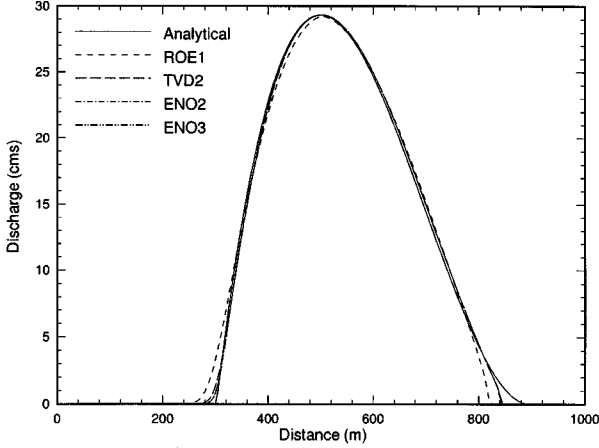
(b) Discharge

Fig. 3. Comparison of idealized dam-break solutions for $h_t/h_r=0.001$ ($t=30$ s).

1-D Transcritical Flow Model



(a) Water depth



(b) Discharge

Fig. 4. Comparison of idealized dam-break solutions for $h_r/h_r=0.0$ ($t=20$ s).

after sudden removal of the dam at the midsection, were computed using the ROE1, TVD2, ENO2 and ENO3 schemes with $\Delta x=5$ m and $C_r=1$. The simulated results and the analytical solutions, at $t=20$ seconds after dam removal, are shown in Fig. 4(a) and (b). The analytical solutions are obtained by using Ritter's method (Henderson, 1966). The TVD2, ENO2 and ENO3 schemes give nearly the same results as the analytical solutions. Since the ROE1 scheme has only first-order accuracy, it again exhibits significant differences, such as those in the front parts of positive and negative waves, between the ROE1 and the other three schemes.

A quantitative comparison of the relative error in the $L2$ norm between the computed results and analytical solutions is shown in Table 1, where the $L2$ norm is defined as

$$L2 = \sqrt{\frac{\sum_{i=1}^{np} (Y_{simulated,i} - Y_{analytical,i})^2}{\sum_{i=1}^{np} (Y_{analytical,i})^2}}, \quad (28)$$

Table 1. $L2$ Norm for Computed Water Depth

| h_r/h_r Scheme | ROE1 | TVD2 | ENO2 | ENO3 |
|------------------|--------|--------|--------|--------|
| 0.001 | 0.0375 | 0.0262 | 0.0252 | 0.0253 |
| 0.0 | 0.0149 | 0.0076 | 0.0068 | 0.0068 |

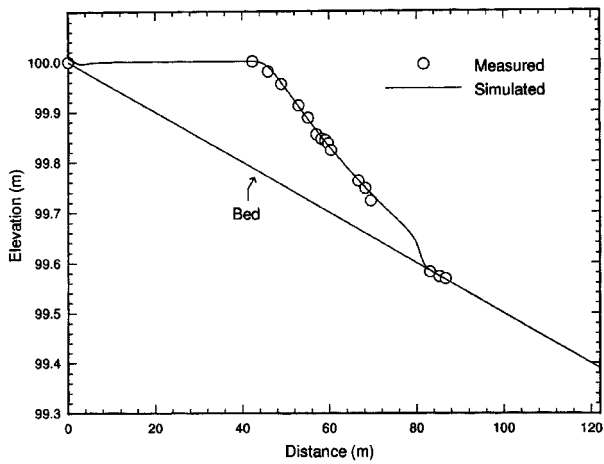
in which np is the grid number. These results indicate that the ENO2 and ENO3 schemes have better accuracy than the other two schemes. The CPU time required is 1 second for the ENO2 scheme, and the computer time is almost equal among the ROE1, TVD2, ENO2 and ENO3 schemes. The second-order ENO scheme is, therefore, proposed for simulation of the transcritical flow when overall accuracy and applicability are considered.

2. Dam-Break Experiment

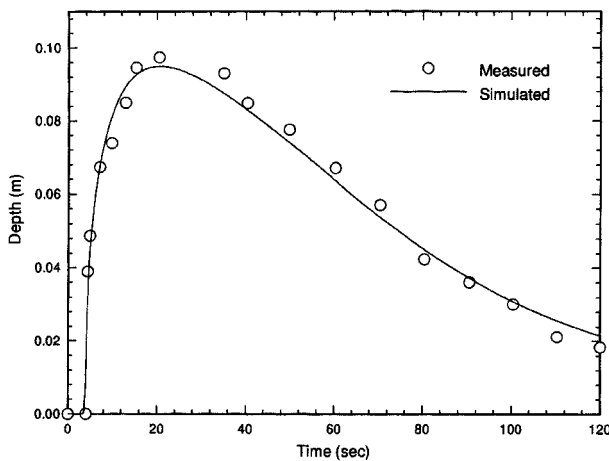
The above test cases only compared simulation results with analytic solutions of idealized dam-break flows. In order to demonstrate that the proposed model is capable of describing a real dam-break scenario, laboratory dam-break experiments carried out at the Waterway Experiment Station (WES), U.S. Corps of Engineers (1960), were also simulated in this study. The experiments were conducted in a rectangular channel with a channel length of 122 m, a width of 1.22 m, a bottom slope of 0.005, and a Manning's roughness coefficient of 0.009. The water depth upstream of the dam was 0.305 m, and the downstream water depth was zero (dry bed). The flow domain was discretized into 122 grids with uniform distribution. Figure 5(a) shows a comparison between the computed and measured water depth variations along the centerline of the flume at time $t=10$ sec. Figure 5(b) and (c) compare the simulated and experimental data at downstream distances of $x=70.1$ m and $x=85.4$ m, respectively. The good agreement between the computed and measured water depth demonstrates that the proposed model is capable of dam-break flow simulation.

3. Pressurization in a Single Pipe

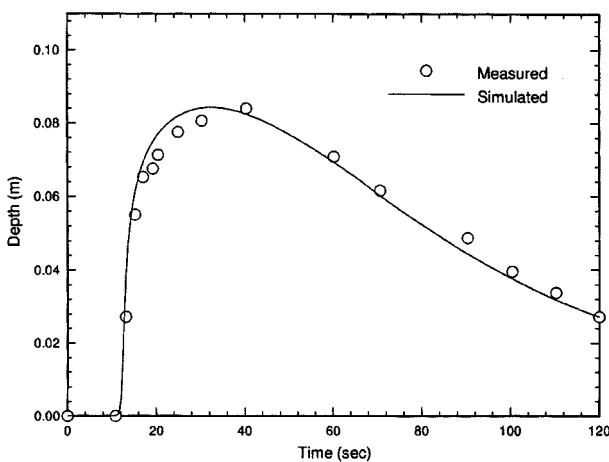
An unsteady free-surface pressurized flow described by Wiggert and Sundquist (1978) was simulated. The length of the horizontal rough pipe was 10 m, the width was 0.51 m, the height was 0.148 m and the Preissmann's slot width above that was $B_s=0.01$ m. A computational grid with $\Delta x=0.125$ m and a Manning's



(a) $t = 10$ s



(b) $x = 70.1$ m



(c) $x = 85.4$ m

Fig. 5. Comparison of dam-break solutions for a WES experiment.

roughness coefficient of $n=0.012$ were used.

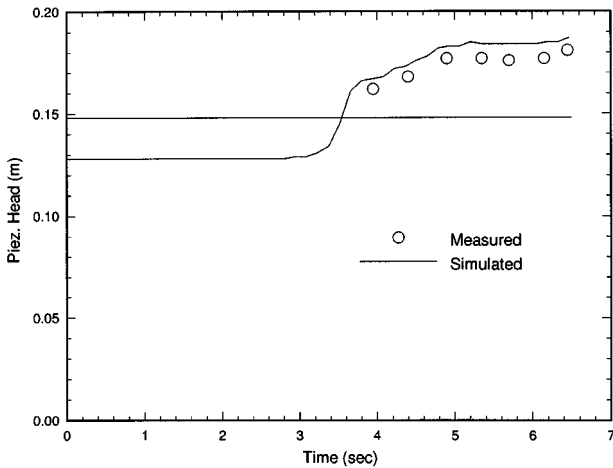
Initially free surface flow conditions with zero discharge and initial water depth=0.128 m were presented. Then a wave coming from the upstream side caused the closed channel to pressurize, starting upstream, and caused an interface separating the pressurized flow from the free surface flow to move downstream. The upstream boundary condition was a given hydrograph, and the downstream boundary condition was a fixed water level equal to 0.128 m. Figure 6(a) and (b) show the results of the variation in time of the water level at $x=3.5$ m and $x=5.5$ m, respectively. The horizontal lines in both figures represent the channel ceiling, and the agreement between the numerical results and the experimental data (Wiggert and Sundquist, 1978) are satisfactory.

4. Idealized Hydraulic Jump

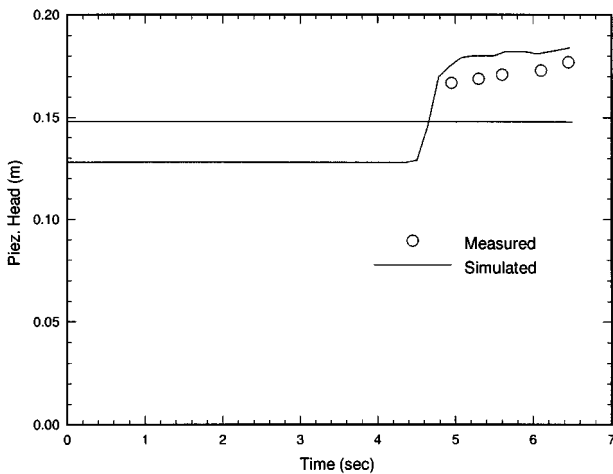
Garcia-Navarro *et al.* (1992) first presented a steady frictionless bell-shaped hump flow, where an analytic solution existed for the analysis of the performance of the algorithm. At the upstream end, a water depth of 9.775 m was imposed while the downstream water depth was held fixed at a value of 7 m. These conditions led to a subcritical accelerating flow before the hump, which reached a critical condition at its top and then became supercritical downhill. A hydraulic jump developed at some location and connected the supercritical profile with the subcritical one imposed by the downstream condition. The steady-state solution obtained from a subcritical initial condition of the linear water surface profile by means of a time-marching procedure using the proposed scheme is presented in Fig. 7(a) along with the analytical solution. The analytical solutions were derived from the conservation of mass and energy combined with the specific force relation (Henderson, 1966). Forty-one uniformly distributed grids with $C_r=1$ were used in this computation. As can be seen, the agreement between the analytical solution and the numerical solution is very good.

Another interesting test case considered by Garcia-Navarro *et al.* (1992) was that of the steady flow across a converging-diverging section in a rectangular, horizontal and frictionless channel. The width variation modified the steady-state profiles as well as those of the propagating fronts. In a 500 m long channel, a sinusoidal width variation was assumed to exist between $x=100$ m and $x=400$ m from a maximum width value of $b=5$ m. A constant discharge at the upstream end was 20 cms, and the downstream water depth was held fixed at a value of 1.8 m. The Subcritical initial condition was started at a linear water surface profile, and the steady-state solution obtained by means of a

1-D Transcritical Flow Model



(a) $x = 3.5$ m



(b) $x = 5.5$ m

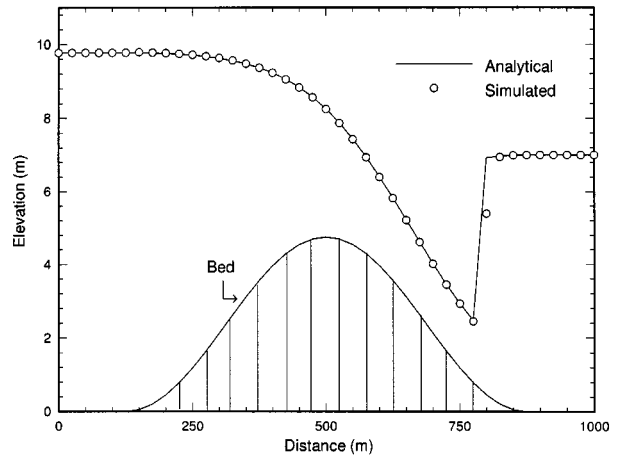
Fig. 6. Pressurization wave in a single pipe.

time-marching procedure using 51 uniform grids is shown in Fig. 7(b) along with the analytical solution. The result produced the water accelerated as it approached the point of maximum contraction ($b_c = 3.587$ m in this example), the flow became critical there, then the flow changed to supercritical and a hydraulic jump formed and connected with the subcritical downstream condition. It is evident that the proposed scheme causes the numerical solution to closely follow the analytical solution while avoiding oscillations.

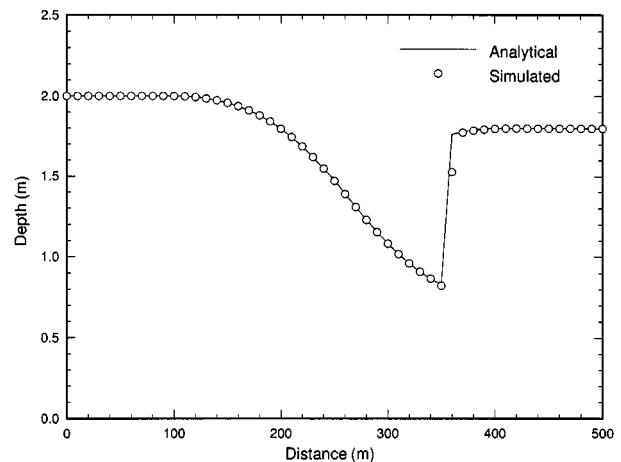
5. Hydraulic Jump Experiments

Considering the many applications of the hydraulic jump, it is desirable that a general-purpose numerical model be found that is capable of solving this

problem. To demonstrate the shock-capturing capability of the proposed model, the computed results were compared with laboratory measurements obtained by Gharangik and Chaudhry (1991) for a 13.9 m long, straight, horizontal, rectangular channel with a upstream Froude number of $F_r = 4.23$ and 6.65. The Manning's roughness coefficient n was reported to range from 0.008 to 0.011 for the six tests conducted. When the numerical model was applied the grid size was 0.3 m, C_r was 1, and a Manning's roughness coefficient n of 0.009 was adopted. For the case of $F_r = 4.23$, the upstream flow discharge and depth were set at 0.053 cms and 0.043 m, respectively, while the downstream depth was set at 0.222 m. The upstream flow discharge and depth were 0.035 cms and 0.024 m for the $F_r = 6.65$ case, respectively, while the downstream depth was 0.195 m. Figure 8(a) and (b) dem-

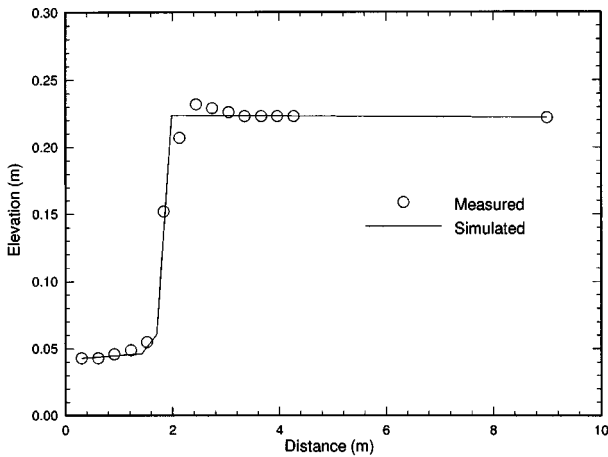


(a) Flow over a hump

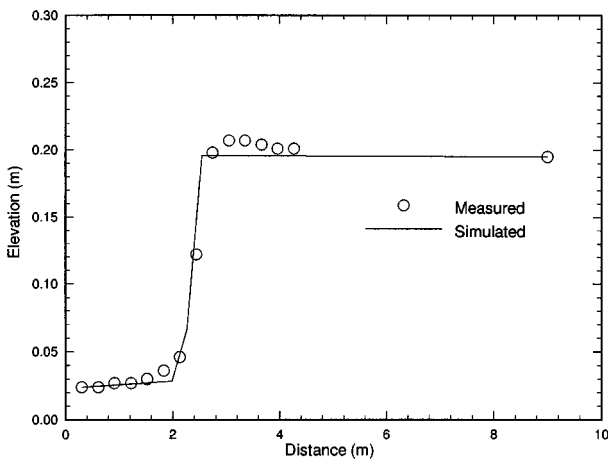


(b) Flow in a converging-diverging channel

Fig. 7. Comparison of solutions for an idealized hydraulic jump.



(a) $F_r = 4.23$



(b) $F_r = 6.65$

Fig. 8. Comparison of solutions for hydraulic jump experiments.

onstrate that the proposed model reproduced the experimental data accurately.

6. Discontinuous Steady Flow over a Ladder of Weirs

This test example involved computation of the discontinuous stationary flow in a 500 m long rectangular channel 6 m wide that contained three identical weirs of 0.25 m in height. The bottom slope was $S_0 = 0.008$, and the Manning’s roughness coefficient was $n = 0.015$. The discharge was 20 cms, and the initial water depth was 2 m. For the flow over the internal weirs, the characteristic equations together with mass continuity and a rating curve for weir flow were used. The proposed model located the sharp discontinuities of the corresponding stationary solution, thus prevent-

ing the appearance of oscillations around them. The results of calculation carried out using the proposed scheme on a $\Delta x = 10$ m grid with $C_r = 1$ are shown in Fig. 9. The proposed model showed good performance in the presence of sharp jumps in the steady-state solution while avoiding oscillations. This model also could efficiently deal with multiple hydraulic jumps for steady flow over a ladder of weirs. The computed result compares favorably with the numerical solution obtained by Garcia-Navarro *et al.* (1992).

V. Conclusions

In this study, a general-purpose mathematical model was developed to solve one-dimensional shallow water flow equations. The model is based on high-resolution non-oscillatory shock-capturing explicit schemes, including a first-order Roe scheme, second-order TVD and ENO schemes, and a third-order ENO scheme.

The model has been applied to a wide variety of hydraulics problems, including dam-break flows under both wet and dry bed conditions, pressurization in a single pipe, a hydraulic jump application and discontinuous steady flow over a ladder of weirs. For each of these cases, the computed results have been compared with analytical solutions, experimental data or other numerical solutions. The agreement between the computed results and experimental measurements or analytical solutions has been found to be satisfactory.

It is evident that the proposed transcritical flow model can be successfully applied to a wide variety of hydraulics problems, especially flows with steep gradient and strong shock features. The proposed model is a significant improvement over most of the existing models that have been developed to solve only the

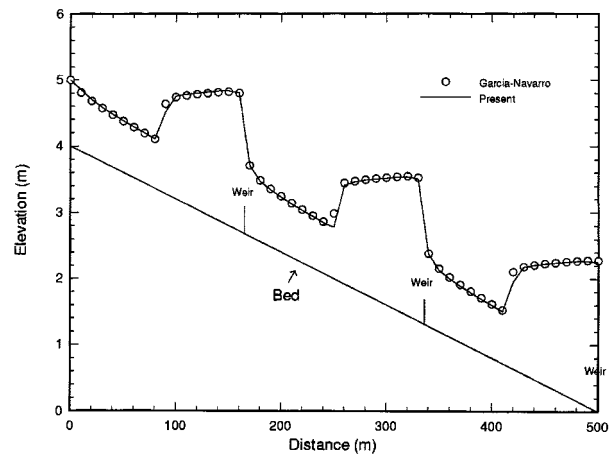


Fig. 9. Computed discontinuous steady flow over a ladder of weirs.

1-D Transcritical Flow Model

gradually varied flow problem.

Acknowledgment

The computer facilities and office provided for this study by the National Center for High-Performance Computing (NCHC) were greatly appreciated. Thanks are also extended to Dr. C. A. Hsu for many helpful discussions.

References

- Alcrudo, F., P. Garcia-Navarro, and J. M. Saviron (1992) Flux difference splitting for 1-D open channel flow equations. *Int. J. Numer. Methods in Fluids*, **14**,1009-1018.
- Baines, M. J., A. Maffio, and A. Di Filippo (1992) Unsteady 1-D flows with steep waves in plant channels: the use of Roe's upwind TVD difference scheme. *Advances in Water Resources*, **15**, 89-94.
- Cunge, J. A., F. M. Holly, and A. Verwey (1980) *Practical Aspects of Computational River Hydraulics*. Pitman Publishing Limited, London, London, U.K.
- Fennema, R. J. and M. H. Chaudhry (1987) Simulation of one-dimensional dam-break flows. *J. Hydr. Res.*, **25**(1), 25-51.
- Fennema, R. J. and M. H. Chaudhry (1990) Explicit methods for 2-D transient free-surface flows. *J. Hydr. Engrg., ASCE*, **116**(8), 1013-1034.
- Garcia-Navarro, P. and J. M. Saviron (1992) McCormack's method for the numerical simulation of one-dimensional discontinuous unsteady open channel flow. *J. Hydr. Res.*, **30**(1),95-105.
- Garcia-Navarro, P., F. Alcrudo, and J. M. Saviron (1992) 1-D open-channel flow simulation using TVD-McCormack scheme. *J. of Hydr. Engrg., ASCE*, **118**(10), 1359-1372.
- Gharangik, A. M. and M. H. Chaudhry (1991) Numerical simulation of hydraulic jump. *J. Hydr. Engrg., ASCE*, **117**(9),1195-1211.
- Glaister, P. (1988) Approximate Riemann solutions of the shallow water equations. *J. Hydr. Res.*, **26**(3), 293-306.
- Harten, A. (1983) High resolution schemes for hyperbolic conservation laws. *J. Comput. Physics*, **49**, 357-393.
- Harten, A. and J. M. Hyman (1983) Self adjusting grid method for one-dimensional hyperbolic conservation laws. *J. Comput. Physics*, **50**, 235-296.
- Harten, A. and S. Osher (1987) Uniformly high-order accurate non-oscillatory schemes I. *SIAM J. Numer. Analysis*, **24**(2), 279-309.
- Henderson, F. M. (1966) *Open Channel Flows*. Macmillan, New York, NY, U.S.A.
- Hsu, C. A. (1995) Unsteady open-channel flow simulation using ENO schemes. *3rd Nat. Conf. Compu. Fluid Dynamics*, pp. 111-120. Nanton, Taiwan, R.O.C.
- Jha, A. K., J. Akiyama, and M. Ura (1995) First and second-order flux difference spilling schemes for dam-break problem. *J. Hydr. Engrg., ASCE*, **121**(12), 877-884.
- Jin, M. and D. L. Fread (1997) Dynamic flood routing with explicit and implicit numerical solution schemes. *J. Hydr. Engrg., ASCE*, **123**(3),166-173.
- Liggett, J. A. and J. A. Cunge (1975) Numerical methods of solutions of the unsteady flow equations. In: *Unsteady Flow in Open Channels*, Chap. 4. Mahmood and Yevjevich Eds. Water Resource Pub., Fort Collins, CO, U.S.A.
- Meselhe, E. A., F. Sotiropoulos, and F. M. Holly, Jr (1997) Numerical simulation of transcritical flow in open channels. *J. of Hydr. Engrg., ASCE*, **123**(9), 774-783.
- Nujic, M. (1995) Efficient implementation of non-oscillatory schemes for the computation of free-surface flows. *J. Hydr. Res.*, **33**(1), 101-111.
- Roe, P. L. (1981) Approximate Riemann solvers, parameter vectors, and difference schemes. *J. Comput. Physics*, **43**, 357-372.
- Stoker, J. J. (1957) *Water Waves*. Interscience Publishers Inc., Wiley and Sons, New York, NY, U.S.A.
- Strang, G. (1968) On the construction and comparison of difference schemes. *SIAM J. Numer. Analysis*, **5**, 506-517.
- Tseng, M. H. (1999) Explicit finite-volume non-oscillatory schemes for 2D transient free surface flows. *Int'l J. Numer. Methods in Fluids*, (in press).
- U.S. Corps of Engineers (1960) *Flood Resulting from Suddenly Breached Dams*. Miscellaneous paper 2(374), Report 1, U.S. Army Engineer Waterways Experiment Station, Corps of Engineers, Vicksburg, MS, U.S.A.
- Wiggert, D. C. and M. J. Sundquist (1978) Fixed-grid characteristics for pipeline transients. *J. Hydr. Engrg., ASCE*, **103**,1403-1415.
- Yang, J. Y., C. A. Hsu, and C. H. Chang (1993) Computation of free surface flows. *J. Hydr. Res.*, **31**(1), 19-34.

一維穿臨界渠道水理模式之驗證

曾明性

行政院國家高速電腦中心工程應用二組

摘 要

穿臨界流場可發生在明渠水路或暗渠涵管中，是水利工程師常會面臨的問題。由於其流場中含有高梯度及不連續之水理特性，較單一流況之超臨界或亞臨界流場複雜甚多，傳統之數值算則通常無法有效處理此類問題。本文應用高解析、不震盪具震波捕捉能力之Roe/TVD/ENO顯式差分算則，進行一維非恆定淺水方程式之離散化，並配合運算元分離法處理源項，同時使用特徵線法處理邊界條件，建立一維穿臨界水理演算模式。本文主要研究目的為應用一系列具數學解析解或水槽試驗資料之水利問題，廣泛進行此一維水理模式之模擬驗證。驗證結果顯示，本研究建立之一維非一定穿臨界水理演算模式，可相當成功地自動處理超臨界、亞臨界及穿臨界等流況之模擬演算，是一個進行水利工程相關問題研究時，有效且頗具信賴度之分析模擬工具。